


ORIGINAL ARTICLE OPEN ACCESS

Large-Scale Physical Model Test on the Influence of Landslide Hazards on Oil and Gas Pipeline Bending

Xianjie Hao^{1,2,3,4} | Yuguang Chen⁴  | Yulong Chen⁴ | Daiyu Gao⁴ | Qian Zhang⁴ | Yinpen Zhao⁴ | Fan Cui^{2,5} | Honglan Zhang⁶

¹Inner Mongolia Research Institute, China University of Mining and Technology (Beijing), Ordos, Inner Mongolia, China | ²Mine Water Protection, State Key Laboratory of Water Resource Protection and Utilization in Coal Mining, Beijing, China | ³Key Laboratory of Safety and High-Efficiency Coal Mining, Ministry of Education (Anhui University of Science and Technology), Huainan, Anhui, China | ⁴School of Energy and Mining Engineering, China University of Mining and Technology (Beijing), Beijing, China | ⁵State Key Laboratory of Coal Resources and Safe Mining, China University of Mining & Technology (Beijing), Beijing, China | ⁶Aviation Security Management Department (Internal Security Department), Beijing Daxing International Airport, Beijing, China

Correspondence: Fan Cui (cuifan@cumtb.edu.cn) | Yuguang Chen (1423291704@qq.com)

Received: 30 March 2024 | **Revised:** 26 October 2024 | **Accepted:** 4 November 2024

Funding: This work is supported by China University of Mining and Technology (Beijing) Inner Mongolia Research Institute Achievement Transformation Project (No. IMRI23008) and the Open Fund of State Key Laboratory of Mining Response and Disaster Prevention and Control in Deep Coal Mines (SKLMRDPC21KF02).

Keywords: landslide geological hazards | oil and gas pipeline | physical model test | pipeline bending deformation

ABSTRACT

Due to its wide distribution, the long-distance oil and gas pipeline will inevitably pass through the landslide risk area. This study aims to investigate the impact of landslide geological disasters on oil and gas pipelines, particularly focusing on the deformation characteristics of pipelines under various landslide dip angles. To achieve this, a large physical simulation platform was designed and established as part of the methods used to replicate the effects of landslide geological disasters on oil and gas pipelines. Experiments were conducted at different dip angles, monitoring and analyzing changes in stress and strain within the pipeline, as well as soil displacement. Based on the experimental results, we draw the following conclusions: (1) the bending process of the pipeline can be divided into slow-bending stage, constant-speed bending stage, and accelerated-bending stage. (2) The tensile strain is produced back to the impact direction of landslide; the compressive strain is produced facing the direction of landslide. At the point with the largest impact force of the landslide, when the dip angle of the landslide is 38°, the rate of slow increase is the greatest in the four stages, which is about 77 times that at a slope of 10° (3) At the same point, with the increase of the dip angle, stress is also gradually increasing. When the slope reaches the angle posing a landslide hazard, the maximum rate of change of stress is about 26.9×10^{-6} kPa/s. (4) At the centre of the pipeline, the strain difference between the back and facing the direction of the landslide increases continuously. These experimental results have obtained the pipeline deformation law in the whole process of pipeline landslide disaster, which can provide great help for the monitoring and early warning of pipeline landslide disasters on site.

1 | Introduction

China's energy industry and energy transportation industry are currently in the process of rapid development. The demand for

oil and gas energy is increasing. As one of the most important means of transportation energy, oil and gas pipeline needs to be paid more attention [1–3]. Due to the large number of oil and gas pipeline construction stations, long lines and wide areas,

This is an open access article under the terms of the [Creative Commons Attribution](https://creativecommons.org/licenses/by/4.0/) License, which permits use, distribution and reproduction in any medium, provided the original work is properly cited.

© 2025 The Author(s). *Energy Science & Engineering* published by Society of Chemical Industry and John Wiley & Sons Ltd.

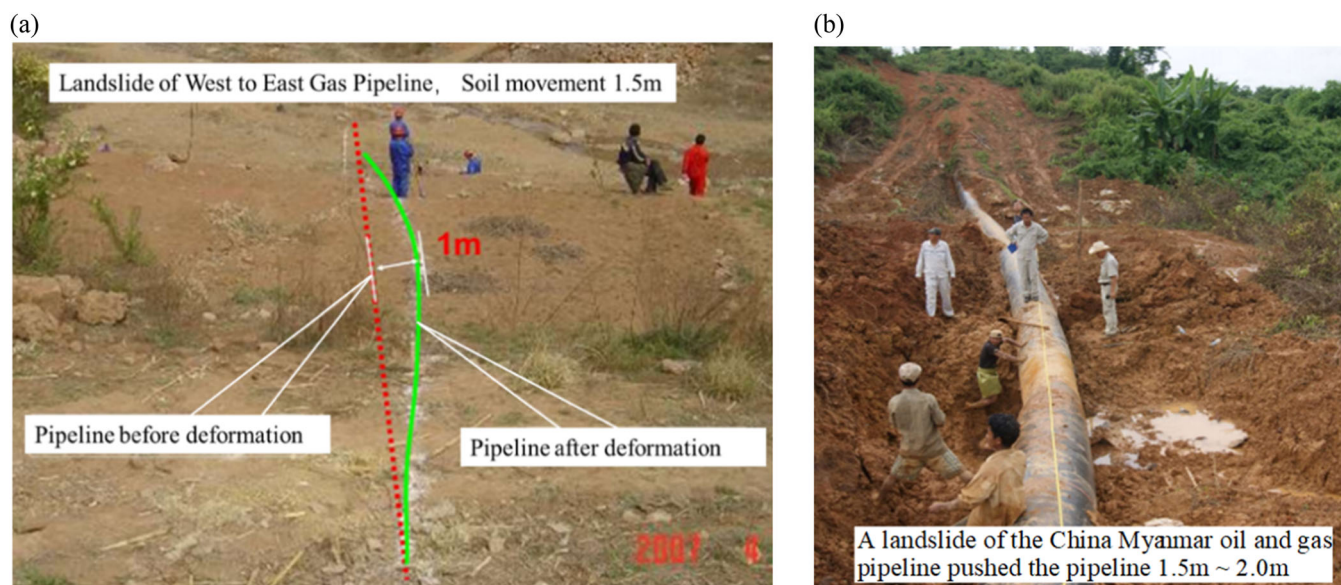


FIGURE 1 | Site of pipeline-landslide hazards: (a) Bending deformation of the west-east natural gas pipeline. (b) Landslide movement of China-Myanmar oil and gas pipeline.

and the increasing mileage in recent years, it is inevitable to cross some landslide disaster risk areas, resulting in geological disasters becoming one of the biggest threats to pipeline safety. For example, the west-east pipeline crosses one of the serious sections in the disaster prone areas in the loess region, and the pipe bending deformation displacement 1 m caused by the regional slope creep (Figure 1A). Another example is that China-Myanmar oil and gas pipeline crosses the Yunnan Guizhou Sichuan region in the southwest, and degradation landslide disaster in accumulation layer occurs, causing the pipeline to move 1.5–2.0 m, as shown in Figure 1B. It can be seen that landslide geological disasters do great harm to oil and gas pipelines, which not only affect the normal operation of oil and gas pipelines, also cause great losses of life and property.

The analysis of pipeline landslide disaster mechanism and failure mode is the focus of current research. On the one hand, it is based on pipeline stress-strain analysis. Due to the limitations of on-site pipeline monitoring [4] and the size effect of the simulation test, the research method of analyzing pipeline stress-strain based on mathematical model is frequently used. Many scholars establish the strain characteristic model of pipeline deformation [5], Constitutive model [6, 7], finite element model [8–13], etc. to analyse the deformation rate, stress-strain and main failure modes of the pipeline under the action of landslide, and estimate the failure probability of the pipeline [14]. It provides technical support for safety assessment and standard formulation of buried pipelines.

However, mathematical model analysis needs physical model test verification, and the two should be closely linked. Physical model test is one of the important means to simulate the deformation and failure process of landslides and reveal the disaster mechanism of landslides. Under the condition of satisfying the similarity theory, selecting the most suitable similar material can grasp the mechanical characteristics and deformation trend of soil and pipeline from the overall situation.

Many scholars studied the deformation mechanism and development trend of landslides through the method of physical model [15–19], but there are few studies on pipeline response under landslide disaster based on physical model. Some scholars [20, 21] studied the mechanical properties, stress distribution and slope failure mode of buried pipeline under soil pipeline interaction through centrifuge physical model test. Most of the experimental studies are based on small-scale model experiments. There are some problems in the experimental methods, such as difficulty in making similar materials and model distortion. In addition, since the reliable relationship between pipeline stress-strain and surface displacement will be the basis for experienced experts to make rapid judgments in pipeline risk assessment, some scholars [22–24] carried out research on landslide surface deformation based on field measurement, and found a rapid assessment method by monitoring the displacement of deep and shallow layers of landslide surface, interpreting the characteristics of displacement curve, establish the relationship between surface deformation and pipeline stress, but due to the large amount of field measurement and difficult data monitoring, the research means of field measurement are also less applied. Many scholars [25, 26] have used numerical simulation to establish a coupled model to analyse the ultimate bearing capacity and stress distribution of buried natural gas pipelines under different working conditions. Some scholars [27] have proposed a quantitative assessment model to analyse the historical landslide disaster data along the oil and gas pipeline to assess the impact of landslides on the risk of long-distance pipelines. Liao et al. [28] simulate the whole process of pipeline-soil interactions between a landslide and a gas pipeline to investigate how pipeline internal pressure, landslide displacement, crack depth ratio and crack aspect ratio influence the J-integral of a circumferential crack in the pipeline under landslide impact. Zhang et al. [29] construct a comprehensive explanatory framework for landslide susceptibility evaluation models to analyse the regional characteristics and spatial heterogeneity of landslide influencing factors, and

discuss the heterogeneity of the generalizability of the models under different landscapes. Liao et al. [30] establish a model of pipeline with defects crossing landslide to analyse the effect of the depth, number and spacing of pipeline defects and gas pressure on the mechanical behaviour of pipeline.

But there is little research on the interaction between landslide and pipeline by using physical model. In this paper, by means of large-scale physical model test, a physical model is constructed by a certain similarity ratio to simulate the interaction between the landslide and the oil and gas pipeline. The strain gauge, micro pressure box and other monitoring equipment are used to quantitatively analyse the stress and strain changes of the oil and gas pipeline buried in the slope under the influence of landslide. Combined with the strain-angle-time relationship, the overall change process of the pipeline is discussed and analysed, and compared with the push curve of the pipeline in the landslide site. The research results can provide theoretical basis for the early warning and prevention and control of oil and gas pipelines under landslide disasters.

2 | Physical Model Device

2.1 | Construction of Experimental Model

In the physical model of landslide geological hazards in oil and gas pipeline, the platform of landslide hazards is simulated with a certain similarity ratio, and the intensity of landslide hazards is simulated by adjusting the height of the landslide-prone slope. Meanwhile, oil and gas pipelines are simulated with the same similarity ratio, and placed on the slope of landslide, and then the influences of landslides on the oil and gas pipeline are studied. In this physical model, on the one hand, the formation

conditions and movement characteristics of landslides can be simulated. On the other hand, the influences of landslide occurrence and development process on the oil and gas pipeline are studied: the relationships between landslide slope, height, rainfall intensity, and stability of the oil and gas pipeline are derived, to lay a foundation for the stable operation of long-distance oil and gas pipelines. This time the influence of the increasing landslide angle on the buried pipeline is studied by this physical model test.

A loading platform, a data acquisition system, and a pipeline system are included in the experimental platform. The lifting and lowering of the jack is controlled by an angle control device to adjust the inclination of the platform. The side of the platform is a measuring point plate with holes, which is used to place experimental pipes, arrange test equipment on the pipes, connect the data analysis platform, and obtain data (Figure 2).

The loading platform is used to build and load the whole experimental instrument with the loading platform of 7.5 m in length, 3 m in width, and 1 m in height. The lifting platform that has an adjustable slope and is 5.5 m in length and 3 m in width is placed on the loading platform with a maximum height of 6.07 m. The height and slope can be adjusted by hydraulic jack. To ensure that the slope will not cause damage to the ground after sliding, a buffer platform is established, with a length of 2 m and a width of 3 m. A 4 m long PVC pipeline was selected, with a buried depth of 60 cm, and was buried in the middle of the slope, 3 m from the top of the slope. It passes closely through the reserved holes in the platform side shield. Both ends of the pipeline are fixed on side baffles to ensure that there will be no significant axial displacement of the pipeline when it is affected by landslides, and only the deflection will be changed, which is more in line with the actual situation of long

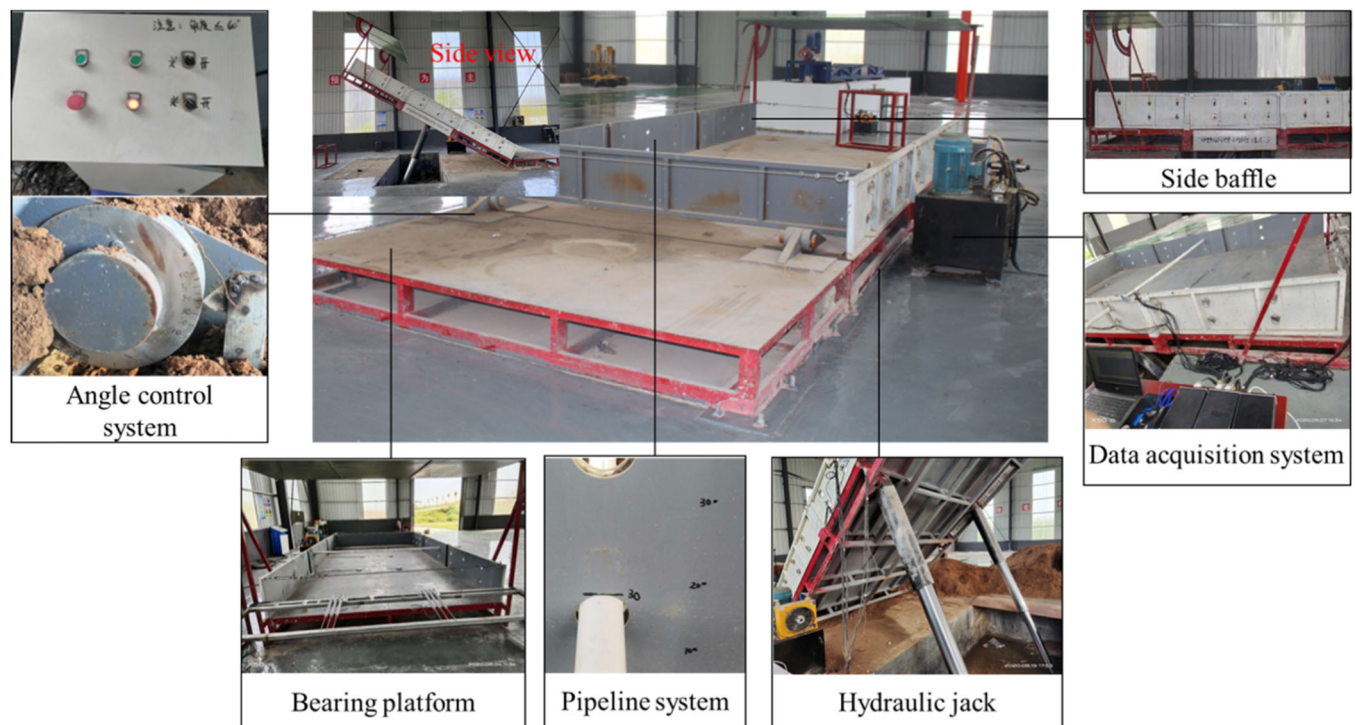


FIGURE 2 | The large-scale physical model for the influence of landslide disaster on oil and gas pipeline bending.

TABLE 1 | Various mechanical parameters of model slope, pipeline and field prototype.

		Experimental slope	Prototype slope	Experimental pipeline	Prototype pipe
Geometric parameter	Size (mm)	5500 × 3000 × 1000	110,000 × 60,000 × 20,000	4000	8,128,000
	Buried depth (mm)	∕	∕	600	1200
	Internal diameter (mm)	∕	∕	50	1016
Physical parameters	Density (g cm ⁻³)	1.80	2.06	6.0	7.80
	Cohesion (kPa)	20.3	466.2	∕	∕
	Internal friction angle (°)	14.6	14.6	∕	∕
	Poisson's ratio	0.65	0.65	0.32	0.42
	Compressive strength (MPa)	2.39	55	0.4	10
	Tensile strength (MPa)	0.09	2.07	32.7	860
	Elastic modulus (MPa)	∕	∕	1300	30000

oil and gas pipelines suffering from landslides on the site. The positional relationship and dimensions between the pipeline and the experimental platform are shown in the following figure.

The physical model test in this article is based on the Froude similarity standard, and the geomechanical model test must comply with relevant similarity standards. Among them, the strength standard is the most important:

$$C_{\sigma} = C_{\rho} \times C_l \times C_g, \quad (3.1)$$

where C_{σ} represents the ratio of the compressive strength of the model material to the compressive strength of the prototype material; C_l represents the ratio of model geometry to prototype geometry; C_{ρ} Represents the ratio of the density of the model material to the density of the prototype material; C_g represents the ratio of the model gravity acceleration to the prototype gravity acceleration.

Because the prototype slope size is 110,000 mm × 60,000 mm × 20,000 mm, experimental slope size 5500 mm × 3000 mm × 1000 mm, so the geometric similarity ratio of soil mass is determined to be 0.05. Because the indoor test and field test are conducted in the same gravity field, $C_g = 1$. According to formula 1, the model material must meet $C_{\sigma} = C_l \cdot C_{\rho}$. According to the density of materials used in the simulation test and the density of rock in the field, the density ratio can be determined as 0.87. The similarity ratio of other parameters is derived: cohesion similarity ratio $C_c = 0.0435$, compressive strength similarity ratio $C_f = 0.0435$, internal friction angle similarity ratio $C_{\varphi} = 1$. Poisson's ratio similarity ratio $C_{\mu} = 1$. The relationship between physical and mechanical parameters and geometric parameters of on-site rocks and model materials is shown in Table 1. Similarly, since the diameter of the Myanmar-China oil and gas pipeline on the site is 1016 mm, the wall thickness is 25.4 mm, and the length of the pipeline in the area affected by landslide disasters is 82.5 m, the pipeline with diameter of 50 mm and length of 4 m is selected according to the experimental conditions, so the geometric similarity ratio is 0.049. The density ratio of 0.77 is determined according to the material density used in the simulation test and the density of oil and gas pipeline on site. Therefore, the similarity ratio of cohesion $C_c = 0.037$, the similarity ratio of tension/pressure $C_f = 0.037$, and the similarity ratio of internal friction angle are derived $C_{\varphi} = 1$. Poisson's ratio similarity ratio $C_{\mu} = 1$. The relationship between physical and mechanical parameters and geometric parameters of on-site oil and gas pipelines and model pipelines is shown in Table 1.

2.2 | Monitoring Equipment Layout

The data acquisition system was used to monitor the landslide and pipeline at the same time, the stress and displacement of landslide mass in the process of landslide deformation were also monitored, and the surface stress and strain of the oil and gas pipeline during the landslide were measured: the occurrence and development process of landslide hazards and the

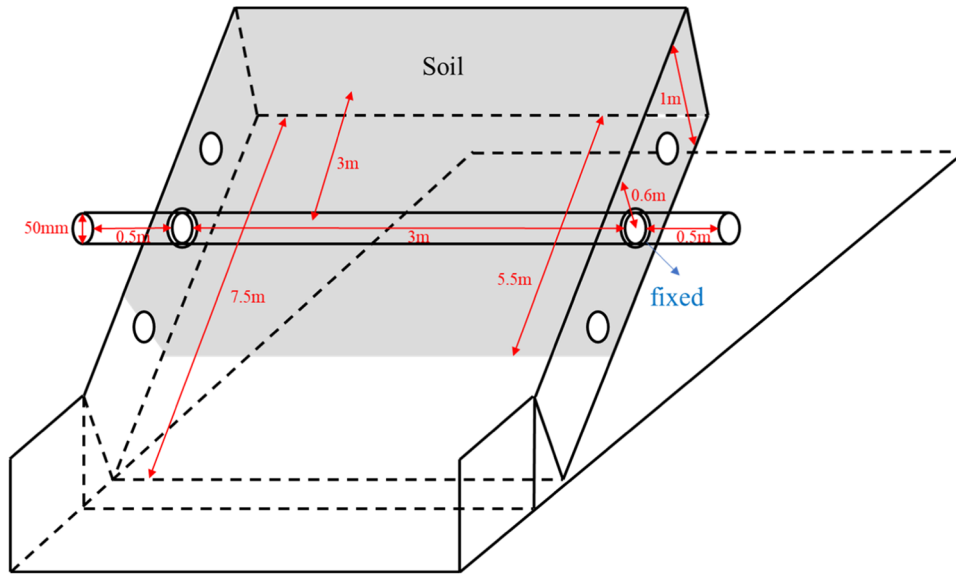


FIGURE 3 | Location relationship between experimental pipeline and slope.

deformation and failure process of oil and gas pipelines were observed by a camera [31].

The PVC pipe is 4 m long, and the width of the slide is 3 m, therefore, a micro-stress box is set at points 1, 2, and 3 m from the left-hand side of the slide. There are two orientations possible for the micro-stress box: facing the impact direction of the landslide or opposite it. In this experiment, a strain gauge should be attached to the surface of the pipe. These strain gauges were used to test the spatio-temporal relationship between pipeline bending and landslide hazards under different dip angles; there are three measuring points with strain gauges on the pipe. Since the length of the pipeline is 3 m, a measuring point with a strain gauge is set every 1 m from the left-hand side of the slide. Each measuring point consists of three strain gauges, which are respectively oriented at 9 o'clock, noon, and 3 o'clock. The surface of the strain gauge is sealed with waterproof adhesive. The actual installation layout of test equipment is shown in Figure 3.

2.3 | Layout of Measuring Points

The stress, strain, and displacement of soil above the pipeline were measured and analysed according to the experimental requirements. The monitoring data were arranged and numbered according to the classification, corresponding to the pipeline stress measuring points and pipeline strain measuring points, respectively (Figures 4 and 5).

2.4 | Experimental Scheme

In this experiment, the influences of landslide geological hazards on oil and gas pipelines were studied under different dip angles. The experiment lasted for 24 h, and the test frequency was 50 Hz. More than 1.1 million experimental data points were obtained from each of the different measuring points. The slope angle of the landslide was simulated by lifting test platform, and

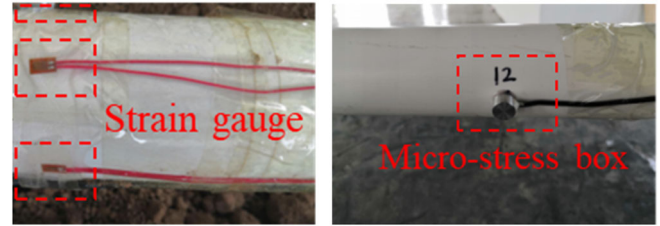


FIGURE 4 | Selection and installation of physical model experiment testing device (micro-stress box, strain gauge).

the slope angle was set to 10°, 20°, 30°, 40°, 50°, and 60°, until the occurrence of a landslide. When the hydraulic jack was not started, the dip angle of the landslide was 0°. During the experiment, the rising height of the hydraulic jack was controlled to control the dip angle of the landslide. Before the rise of the slope, the monitoring equipment was turned on to monitor the stress and strain changes on the pipeline during the increase of the slope and the process of keeping the dip angle unchanged.

3 | Test Results and Analysis

3.1 | Evolution Process of Landslide in Physical Simulation Test

In the whole process of physical model test, the three evolution stages of landslide are simulated by increasing the slope angle: slow creep, creep-slip, accelerated creep and rapid deformation stage [32].

From the macroscopic deformation and failure signs in the physical model experiment, it can be seen that when the landslide angle is 0° to 10°, the soil begins to be compacted gradually, the slope is relatively stable, and there are fine cracks in the front edge of the slope, which belongs to the stage of slow creep; When the landslide angle is from 10° to 20°, the fine cracks on the slope surface gradually expand and extend in the

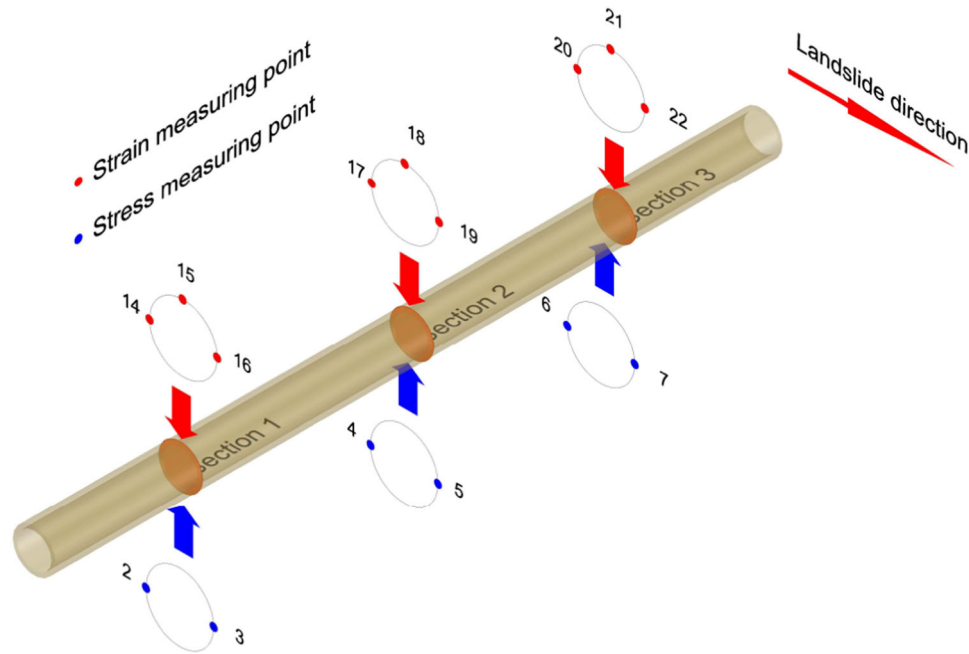


FIGURE 5 | Layout of measuring points for physical model experiment.

horizontal and longitudinal directions. At this time, the landslide is in the stage of uniform creep; When the landslide angle is from 20° to the critical angle (38°), the slope surface of the landslide forms a tension zone, obvious tension cracks appear behind the slope, and shear cracks appear on both sides of the middle and front of the slope, but the fracture system around the landslide has not been trapped, that is, the tension cracks on the top of the slope have not penetrated the whole sliding surface in the water square direction and have not reached the critical sliding stage. Therefore, it can be seen that the landslide is in the accelerated creep stage. When the landslide angle reaches the critical angle, the tension crack at the pipeline passes through the sliding surface to form a complete shear failure surface. It can be seen that the pipeline has the effect of preventing sliding on the slope, and then the overall instability failure is manifested as push type landslide [33]. The landslide is a stage of rapid deformation, and then the soil stress is released rapidly, the slope tends to be stable as a whole, and no new landslide surface appears. During the whole experiment, the angle is raised slowly, and when reaching a certain stage, it is placed continuously to observe the landslide phenomenon, which can simulate the landslide disaster under engineering disturbance. At the same time, about 38° can be used as the critical angle of overall instability and failure of physical model test slope under no rain condition as the experimental reference.

3.2 | Discussion of the Changes in Strain

To study the strain variation of the pipeline, the variations at the same landslide dip angle and different measuring points and the variations at the same measuring point and different landslide dip angles are evaluated. The same dip angle and different measuring points are used to study the bending law of different positions on the pipeline: moreover, the purpose of the same measuring point and different landslide dip angles is to study

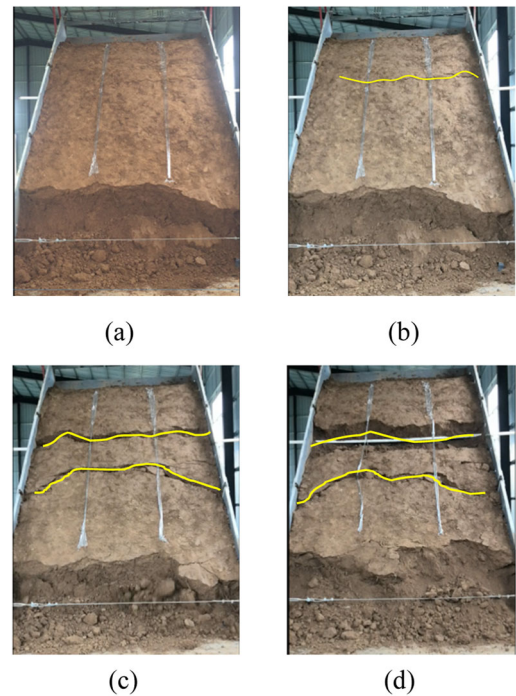


FIGURE 6 | Failure diagram of different stages of landslide in physical model experiment. (a) Slow creep stage, (b) creep-slip stage, (c) accelerated creep, and (d) rapid deformation.

the bending of the pipeline with the change of the landslide dip angle.

3.2.1 | Same Dip Angle, Different Measuring Points

The strain change processes in the direction of 3 o'clock (measuring point 17), 9 o'clock (measuring point 19), and noon (measuring point 18) on the section circumference at the centre

of the pipeline are illustrated in Figure 6: among them, the measuring points in the direction of 3 o'clock are those facing the motion direction of the landslide. It is found that the measuring points in the direction of 3 o'clock produce compressive strain, and the strain decreases. The maximum strain is 248 microstrain. Meanwhile, the measuring points in the direction of noon monitor the strain just above the pipeline cross-section. As can be seen, compressive strain continues to occur at this point, indicating that the point does not experience the pressure facing the direction of motion of the landslide, thus experiencing a lower strain value with a maximum value of 100 microstrain. Its trend is similar to that of the strain variation at the measuring points in the direction of 3 o'clock; the measuring point in the 9-o'clock-direction is facing backwards relative to the impact of landslides. The strain generated at this point is tensile, the pipeline generates a maximum strain value of 750 microstrain, which is much larger than that generated at the point producing a compressive strain. It can also be seen from the figure that the strain changes in the three directions of 3 o'clock (measuring points 14 and 20), 9 o'clock (measuring points 16 and 22), and noon (measuring points 15 and 21) at the bilateral sides of the pipeline are similar to those in the section at the centre of the pipeline. Tensile strain is shown to occur in the left section of the pipeline in the direction of 9 o'clock. Due to the different stress conditions at different locations in the pipeline during the landslide, the law of tensile strain in the direction of 9 o'clock on the left-hand section of the pipeline first increases, and then decreases. This kind of spring-back phenomenon is because the section on the left-hand side of the pipeline is at the boundary of the slide. The slide boundary has a definite restriction effect on the measuring points of the left-hand section of the pipeline, which leads to the decrease of the strain thereat.

3.2.2 | Different Dip Angles at the Same Measuring Point

The overall changes in strain can be divided into three stages, namely, slow-bending stage, constant-speed bending stage, and accelerated-bending stage. When the pipeline is in the lifting stage, the pipeline just begins to bear the sliding force generated by the soil, and the strain produced by the pipeline changes visibly, and the rate of change of strain is fast. The absolute value of strain on the pipeline changes more than in other three stages. In the constant-speed bending stage, the pipeline will still undergo a change in strain due to the increase of the dip angle, and the change is greater than that in the slow-bending stage. When the deformation of the pipeline reaches a certain extent, the pipeline will enter the accelerated-bending stage. At this time, the strain of the pipeline begins to increase sharply, and the pipeline may even buckle. The changes of the three stages are shown in Figure 6. The strain changes of different dip angles of the pipeline at the same measuring point are ascertained here. As shown in Figure 6, the strain variation of the pipeline under different dip angles is analysed by taking the measuring point 19 (subject to the largest impact force of the landslide) as an example. In the process of a landslide, as the dip angle is increased from 0° to 10° , the strain in the pipeline changes abruptly, and the maximum change therein is 550 microstrain. After the dip angle of the landslide reaches 10° . The strain of the pipeline increases slowly at a rate of 1.4×10^{-4} microstrain per second, when the dip angle of the landslide rises to 20° . The strain increases rapidly to 568 microstrain again and then springs back to a certain extent. After the dip angle of the landslide reaches 20° , the strain in the pipeline still increases slowly at the rate of 3.6×10^{-4} microstrain per second. This is about twice the rate of increase when the landslide angle

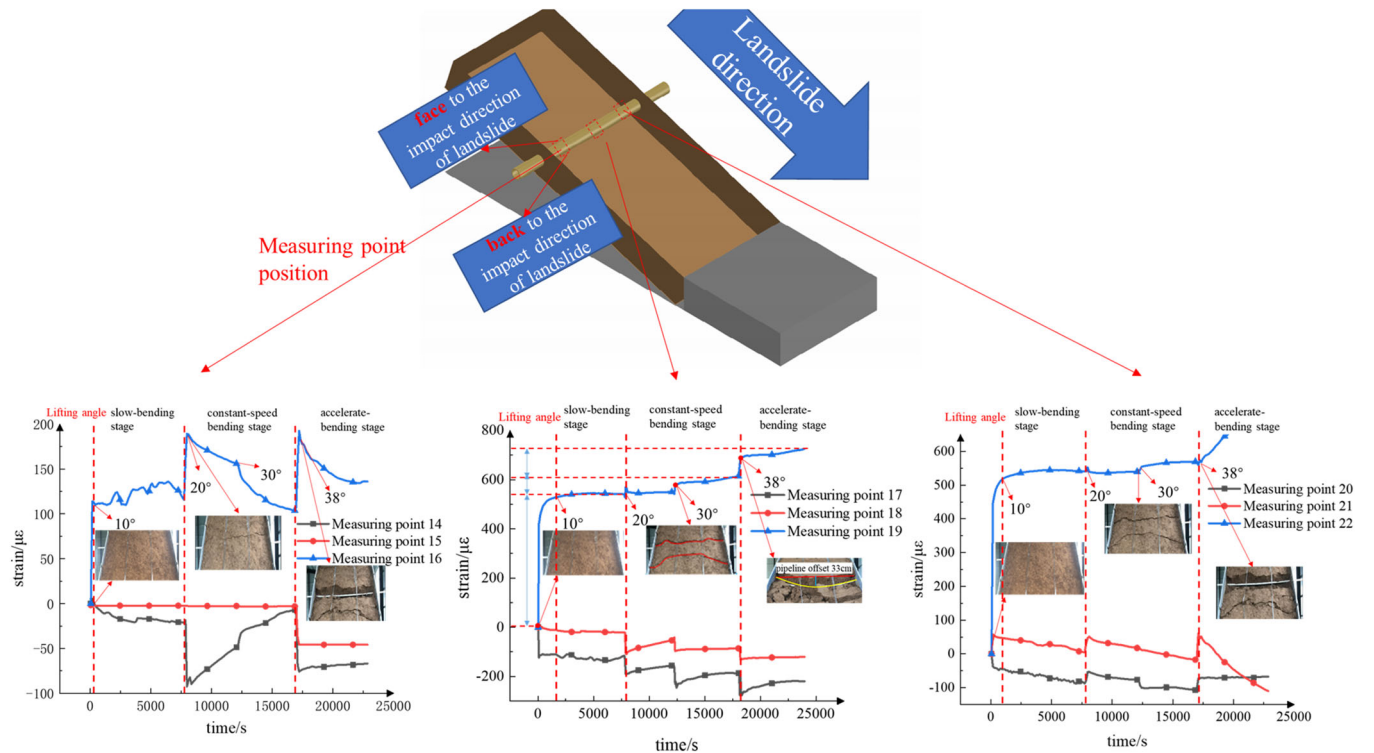


FIGURE 7 | The whole physical simulation test process changes of pipeline in strain.

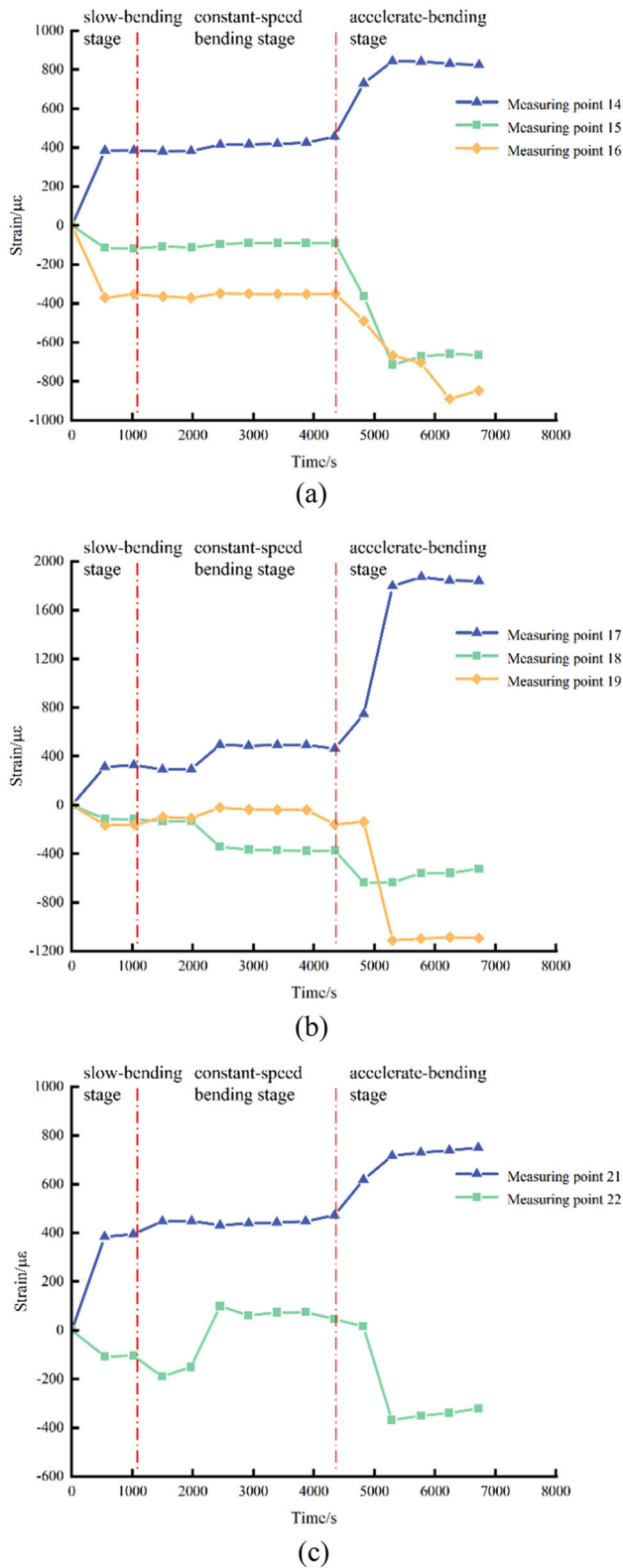


FIGURE 8 | The whole physical simulation parallel test process changes of pipeline in strain. (a) Left end pipe, (b) middle pipe, and (c) right end pipe.

is 10° . When the dip angle rises to 30° , the pipeline strain increases rapidly to 581 microstrain. After the dip angle of the landslide reaches 30° , pipeline strain increases slowly at a rate of 38.8×10^{-4} per second. Compared with the rate of

increase when the dip angle is 20° , the rate of increase at 30° is increased to about 27 times that at a landslide angle of 10° . When the slope angle reaches 38° , a landslide occurs, and the pipeline strain reaches 692 microstrain. Then, the strain of the pipeline increases slowly, and the rate of increase reaches 108×10^{-4} microstrain per second. When the dip angle of the landslide is 38° , the rate of slow increase is the greatest in the four stages, which is about 77 times that at a slope of 10° (Figure 7).

To sum up, according to the analysis of the same measuring point and different dip angles of the pipeline, it is found that the overall change of the pipeline conforms to the proposed staged changes. When raising the slope, the pipeline strain will increase rapidly, but because of its innate characteristics, the pipeline may spring back. However, when the dip angle of the landslide reaches the required dip angle, the pipeline will undergo a slow and stable strain increase due to the downward motion of the soil. In general, with the increase of the dip angle, the rate of slow increase of pipeline strain will also increase.

3.3 | Discussion of the Changes in Stress

Like strain, the stress variations on a pipeline in a landslide are analysed. Herein, the stress variation is investigated from the same landslide angle, different measuring points, and the same measuring point, but at different landslide angles.

3.3.1 | Same Dip Angle, Different Measuring Points

The pipeline is analysed using data from different measuring points with the same dip angle; the pipeline stress measuring points are the left-hand cross-section (measuring points 2 and 3), the central cross-section (measuring points 4 and 5), and the right-hand cross-section (measuring points 6 and 7). Among them, measuring points 2, 4, and 6 are those facing the direction of motion of the landslide, and measuring points 3, 5, and 7 face the opposite way. It can be seen from the figure that the maximum stress variation of the measuring points on the left-hand cross-section increases to 0.4 kPa, that on the right is 0.35 kPa, and that on the cross-section at the centre cross-section reaches 0.43 kPa. The stress variation of the measuring points at the bilateral sides of the pipeline is less than that of the measuring points on the cross-section at the centre of the pipeline. During landslide impact hazards, the cross-section at the centre of the pipeline is subject to the greatest impact load.

According to the analysis of the measuring points at different positions of the pipeline in three different stages, when the pipeline is in the slow-bending stage, similar rules are presented by the stress changes around the cross-section position. The stress change of the measuring point at the left-hand cross-section position is greatest. The maximum stress increases to 0.2 kPa, followed by that at the right (0.14 kPa), and the stress change at the measuring point at the centre cross-section position is the smallest, the maximum stress increases to 0.13 kPa thereat. The reason for this may be that the measuring points at the sides of the pipeline cross-section are located at the

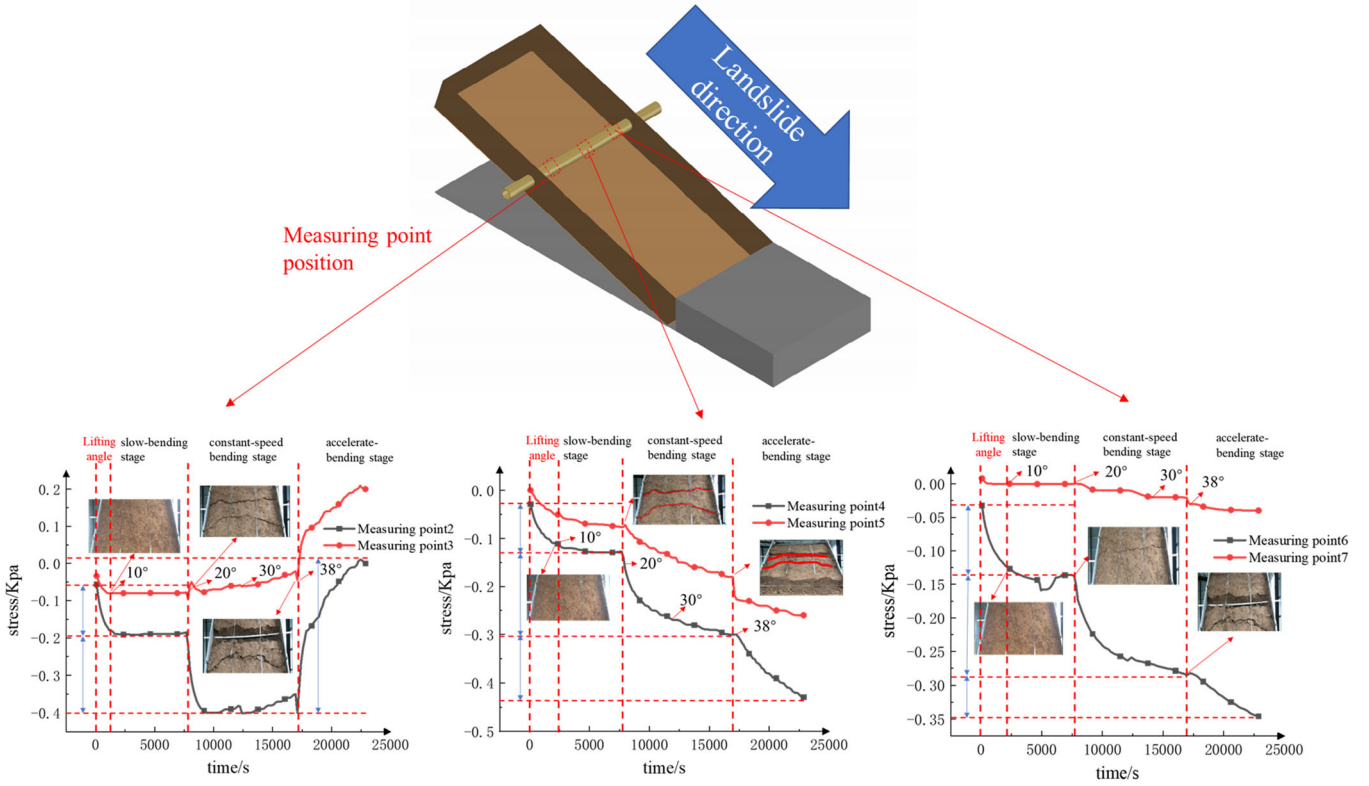


FIGURE 9 | The whole physical simulation test process changes of pipeline in stress.

sides of the sliding mass. More auxiliary forces are generated by the baffles at the bilateral sides of the slideway, resulting in an increase in the force on the measuring points at the sides of the cross-section; when the pipeline is in the constant-speeding bending stage, the pressure increment of all the measuring points increases rapidly, the stress of the left-hand and right-hand sides reaches 0.36 and 0.28 kPa, respectively. The stress on the cross-section at the centre reaches 0.30 kPa. The pressure increment of the measuring point at the left-hand cross-section remains greater than that at the centre, however, the measuring points at the sides of the cross-section experience different degrees of rebound, in which the stress change at the measuring point at the left-hand cross-section is the greatest. The rebound phenomenon is the clearest and when the landslide occurs, the maximum stress on the cross-section at the centre of the pipeline reaches 0.43 kPa, and the maximum stress on the left-hand and right-hand sides of the pipeline is 0.4 and 0.35 kPa, respectively. The stress change at the measuring points at the sides of the pipeline cross-section is less than that at the centre of the pipeline cross-section.

Due to the irregularity of the landslide impact hazard, the stress change at the measuring point on the left exhibits quite particular behaviour: stress spring-back occurs and a certain degree of positive growth is presented therein. At this time, the measuring point on the left side of the cross-section is subject to a large reverse force. The reason for this phenomenon may be that all the soil around the pipeline at the measuring point has slipped, and the force acting on the pipe has almost disappeared. Due to the bending deformation of the pipeline, the measuring point on the left-hand cross-section undergoes a reverse displacement. Therefore, the cross-sectional measuring point is

subject to a reversal of force, resulting in large-scale stress spring-back.

In summary, for the same dip angle and different measuring points, when the landslide hazard occurs, the stress on the cross-section at the centre of the pipeline is the largest, and the stress at the sides is lower. Due to the irregularity of the landslide, there is a certain degree of stress spring-back at the measuring point of the pipeline at the boundary of the sliding mass. If the soil around the measuring point of the pipeline slides away, then the pipeline is not stressed by the soil.

3.3.2 | Same Measuring Point, Different Dip Angles

Under different dip angles of landslides, a similar trend is shown in the stress at each measuring point, therefore, the stress at the same measuring point at different dip angles is analysed by taking measuring point 4 as the object. When the slope angle reaches 10°, the stress on the pipeline increases at a rate of 38.1×10^{-6} kPa/s, and the stress reaches 0.12 kPa. Then the stress on the pipeline increases at about 2.5×10^{-6} kPa/s. With the further increase of the slope angle, the stress change of the pipeline increases; when the dip angle of the landslide reaches 20°, the stress changes at 28.5×10^{-6} kPa/s. When the slope angle reaches 30°, the stress on the pipeline increases at 9.3×10^{-6} kPa/s. When the slope reaches the angle posing a landslide hazard, the maximum rate of change of stress is about 26.9×10^{-6} kPa/s. Although the rate of change of stress is not the most rapid, a state of rapid linear increase is presented by the stress change at the measuring point, and the maximum stress reaches 4.3 kPa.

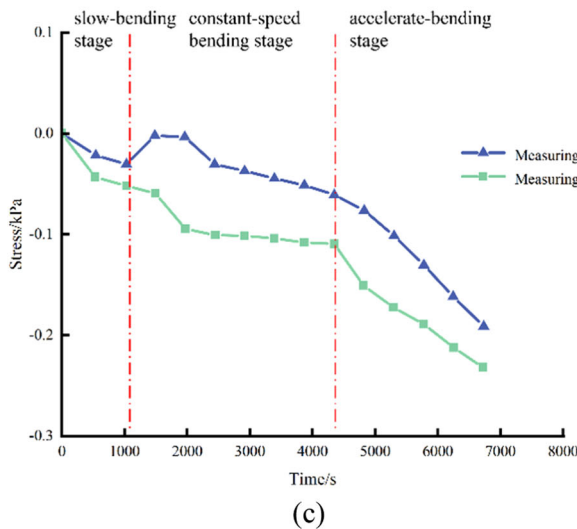
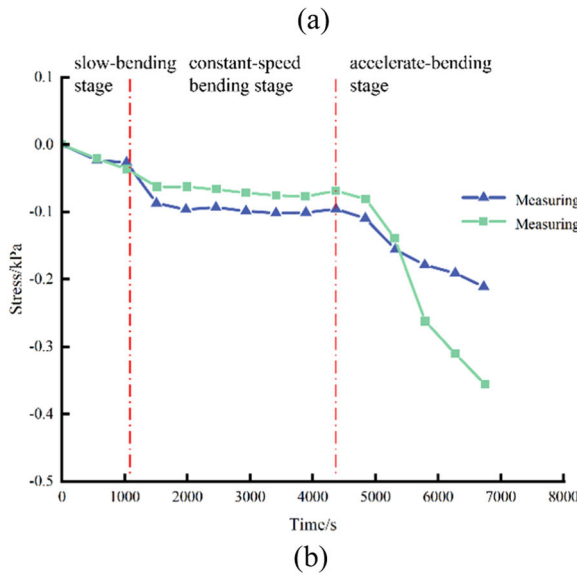
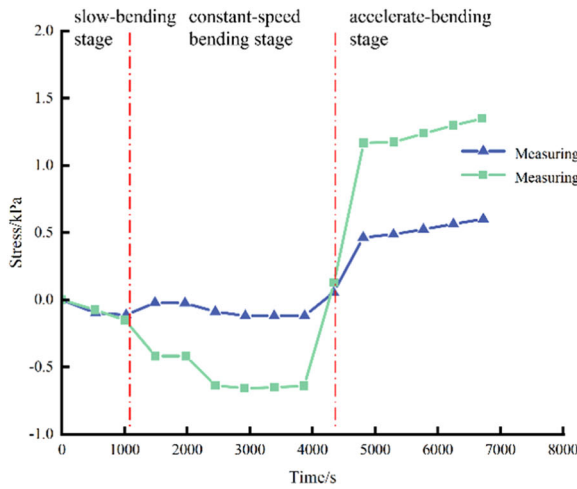


FIGURE 10 | The whole physical simulation parallel test process changes of pipeline in stress. (a) Left end pipe, (b) middle pipe, and (c) right end pipe.

In summary, for the same measuring point, stress increases with the increasing dip angle. When the pipeline is in the slow-bending stage, a slow increase in stress occurs; when the pipeline is in the constant-speed bending stage, the stress

increases rapidly. When the pipeline is in the accelerated-bending stage, the rate of increase of stress is accelerated, and a linear rapid increase in stress occurs until the stress on the pipeline reaches its maximum.

4 | Discussion

In Figure 8, two strain measuring points at 3 o'clock and 9 o'clock on the three sections of the pipeline are selected, respectively (making a total of six points). Through the data from these six measuring points at different landslide dip angles, the pipeline dip diagram was drawn, and the bending deformation degree of the pipeline in the dip angle can be seen more intuitively. The lower curve is plotted using measuring points which face away from the direction of motion of the landslide (and are expressed as a tensile strain curve); the upper curve is plotted from the measuring points which face the impact direction of the landslide (and are expressed as a compressive strain curve). For clarity, the strain is changed to a positive value without changing the incremental compressive strain. When the dip angle of the landslide is increased to 10° , the tensile strain and compressive strain in the pipeline increase significantly. Upon uplift to 20° , the pipeline enters the constant-speed bending stage. Due to its bending resistance, the bending deformation is less than that at a slope of 10° . When the dip angle of the landslide is 30° , the bending deformation is greater than that at 20° . When the landslide occurs, the pipeline enters the accelerated-bending stage. The tensile strain at the centre of the pipeline reaches 210 microstrain, and the change in the tensile strain is greater than that in the compressive strain, however, the variation of tensile strain and compressive strain at the sides of the pipeline is lower, and the variation of compressive strain is 52 microstrain, which is slightly larger than the variation in the tensile strain. Therefore, with the increase of the angle, the strain difference between the point facing the direction of motion of the landslide and that facing the opposite way at the centre of the pipeline is increasing, while the difference in strain between the two points at the two sides of the pipeline is decreasing, the strain is large in the middle and small at the ends, and the form of bending is parabolic. The results are compared with the form of on-site pipeline bending: the experimental results are consistent with those measured in situ (Figures 9–11).

5 | Conclusion

The landslide hazards with dip angles of 10° , 20° , and 30° were investigated: six stress measuring points, nine strain measuring points, and six displacement measuring points were monitored, and the real-time data of the pipeline in the process of the landslide were obtained. The conclusions are as follows:

1. The whole strain change process of the pipeline can be divided into three stages: slow-bending stage, constant-speed bending stage and accelerated-bending stage.
2. In the process of pipeline-landslide hazards, the stress on the section at the centre of the pipeline is the largest for 0.43 kPa, and the maximum stress on the left cross-section

Landslide state in each stage of the experiment

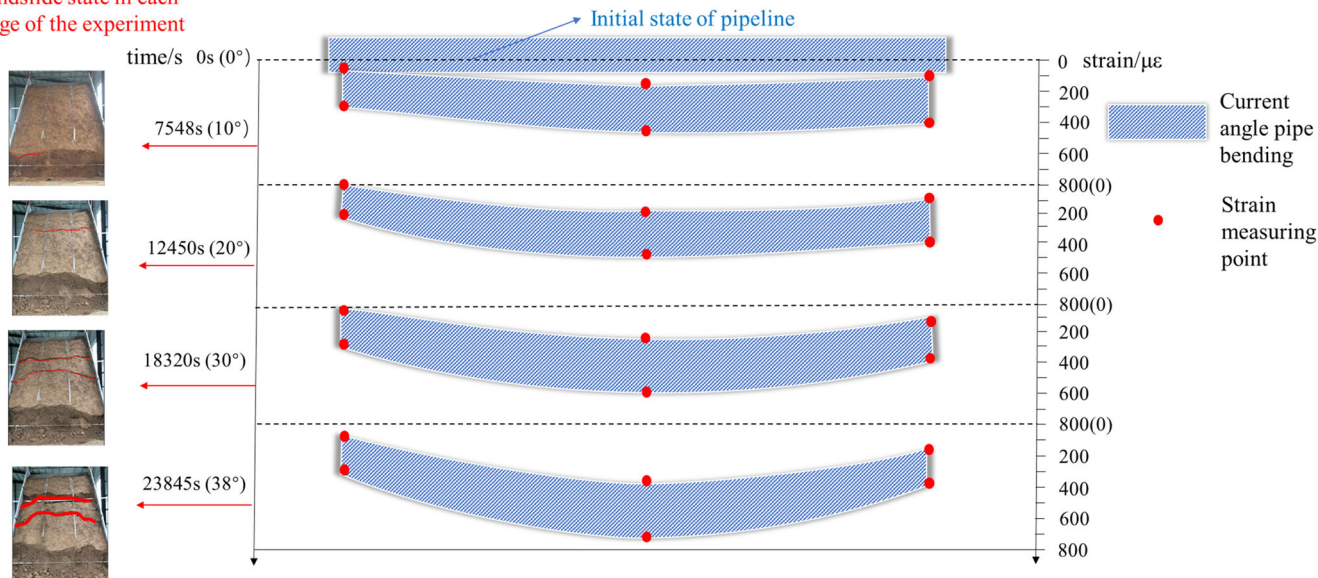


FIGURE 11 | Simulation of changes in a pipeline affected by different landslide angles.

of the pipeline is 0.4 kPa, and the maximum stress on the right cross-section of the pipeline is 0.35 kPa. When the dip angle of the landslide is constant, the point strain in the centre of the pipeline is the largest for 750 microstrain. When the pipeline is subject to a landslide, the point facing the impact direction of the landslide is subject to tensile strain, and vice versa. Moreover, the tensile strain in the pipeline is much greater than the compressive strain, thus the centre of the pipeline is the most readily damaged.

3. With the increase of the dip angle, the strain in the pipeline increases continuously. When the slope angle reaches 38°, a landslide occurs, and the pipeline strain reaches 692 microstrain. Then, the strain of the pipeline increases slowly, and the rate of increase reaches 108×10^{-4} microstrain per second. When the dip angle of the landslide is 38°, the rate of slow increase is the greatest in the four stages, which is about 77 times that at a slope of 10°.
4. At the same point, with the increase of the dip angle, stress is also gradually increasing. When the slope reaches the angle posing a landslide hazard, the maximum rate of change of stress is about 26.9×10^{-6} kPa/s. Although the rate of change of stress is not the most rapid, a state of rapid linear increase is presented by the stress change at the measuring point, and the maximum stress reaches 4.3 kPa.

This study employs on-site measurement methods to collect actual data for research purposes. In the future, numerical models combined with physical models will be used together to analyse the deformation of pipelines under geological disasters, to obtain better and more accurate conclusions and patterns.

Author Contributions

All authors contributed to the study conception and design. Material preparation, data collection and analysis were performed by Hao

Xianjie, Zhang Honglan, Zhang Qian and Zhao Guanghui. The first draft of the manuscript was written by Hao Xianjie, Zhang Honglan and Zhang Qian, and all authors commented on previous versions of the manuscript. All authors read and approved the final manuscript.

Acknowledgements

This work is supported by China University of Mining and Technology (Beijing) Inner Mongolia Research Institute Achievement Transformation Project (No. IMRI23008) and the Open Fund of State Key Laboratory of Mining Response and Disaster Prevention and Control in Deep Coal Mines (SKLMRDPC21KF02).

Conflicts of Interest

The authors declare no conflicts of interest.

References

1. Z. Lin, K. Liu, J. Liu, D. Geng, K. Ren, and Z. Zheng, "Numerical Model for Geothermal Energy Utilization From Double Pipe Heat Exchanger in Abandoned Oil Wells," *Advances in Geo-Energy Research* 5, no. 2 (2021): 212–221.
2. J. Li, Z. Yang, S. Wu, and S. Pan, "Key Issues and Development Direction of Petroleum Geology Research of Source Rock Strata in China," *Advances in Geo-Energy Research* 5, no. 2 (2021): 121–126.
3. A. Choubineh, A. Helalizadeh, and D. A. Wood, "Estimation of Minimum Miscibility Pressure of Varied Gas Compositions and Reservoir Crude Oil Over a Wide Range of Conditions Using an Artificial Neural Network Model," *Advances in Geo-Energy Research* 3, no. 1 (2019): 52–66.
4. D. Sun, H. Wen, Y. Zhang, and M. Xue, "An Optimal Sample Selection-Based Logistic Regression Model of Slope Physical Resistance Against Rainfall-Induced Landslide," *Natural Hazards* 105, no. 2 (2021): 1255–1279.
5. H. Ma, B. He, X. Luo, et al., "Investigation on Strain Characteristic of Buried Natural Gas Pipeline Under Longitudinal Landslide Debris Flow," *Journal of Natural Gas Science and Engineering* 86 (2021): 103708.
6. X. Luo, J. Ma, J. Zheng, and J. Shi, "Finite Element Analysis of Buried Polyethylene Pipe Subjected to Seismic Landslide," *Journal of Pressure Vessel Technology* 136, no. 3 (2014): 031801, <https://doi.org/10.1115/1.4026148>.

7. E. Ruocco, R. Di Laora, and V. Minutolo, "An Exponential Matrix Method for the Buckling Analysis of Underground Pipelines Subjected to Landslide Loads," *Procedia Earth and Planetary Science* 16 (2016): 25–34.
8. M. Bai, Y. Du, Y. Chen, Y. Xing, and P. Zhao, "Risk Assessment of Long Gas and Oil Pipeline Projects Inducing Landslide Disasters During Construction," *Journal of Performance of Constructed Facilities* 31, no. 5 (2017): 04017063.
9. Y. Long and K. Le, "Reliability Analysis of High Pressure Buried Pipeline Under Landslide," *Applied Mechanics and Materials* 2974 (2014): 1081–1086.
10. F. Yuan, L. Li, Z. Guo, and L. Wang, "Landslide Impact on Submarine Pipelines: Analytical and Numerical Analysis," *Journal of Engineering Mechanics* 141, no. 2 (2015): 04014109.
11. J. Zhang, Z. Liang, and C. Han, "Mechanical Behavior Analysis of the Buried Steel Pipeline Crossing Landslide Area," *Journal of Pressure Vessel Technology* 138, no. 5 (2016): 051702.
12. X. Hao, Y. Wei, K. Yang, et al., "Anisotropy of Crack Initiation Strength and Damage Strength of Coal Reservoirs," *Petroleum Exploration and Development* 48, no. 1 (2021): 243–255.
13. S. Masahiro and M. Yoshihisa, "Regional Landslide Susceptibility Following the Mid NIIGATA Prefecture Earthquake in 2004 With NEWMARK'S Sliding Block Analysis," *Landslides* 14, no. 6 (2017).
14. P. A. Juan, C. David, E. Nicolas, et al., "Quantitative-Mechanistic Model for Assessing Landslide Probability and Pipeline Failure Probability Due to Landslides," *Engineering Geology* 222 (2017): 211–224.
15. W. Li, C. Liu, Y. Hong, et al., "Rainstorm-Induced Shallow Landslides Process and Evaluation a Case Study From Three Hot Spots," *Geomatics, Natural Hazards and Risk* 7, no. 6 (2016): 1908–1918.
16. Z. Tao, Y. Shu, X. Yang, Y. Peng, Q. Chen, and H. Zhang, "Physical Model Test Study on Shear Strength Characteristics of Slope Sliding Surface in Nanfen Open-Pit Mine," *International Journal of Mining Science and Technology* 30, no. 3 (2020): 421–429.
17. Z. Wei, D. Wang, H. Sun, and X. Yan, "Comparison of a Physical Model and Phenomenological Model to Forecast Groundwater Levels in a Rainfall-Induced Deep-Seated Landslide," *Journal of Hydrology* 586, no. March (2020): 124894.
18. C. Zhou, X. Hu, W. Zheng, C. Xu, and Q. Wang, "Displacement Characteristic of Landslides Reinforced With Flexible Piles: Field and Physical Model Test," *Journal of Mountain Science* 17, no. 4 (2020): 787–800.
19. J. Gan and Y. X. Zhang, "Analysis of Model Tests of Rainfall-Induced Soil Deposit Landslide," *Advances in Civil Engineering* 2020 (2020), <https://doi.org/10.1155/2020/6431247>.
20. W. Zhang and A. Askarinejad, "Behaviour of Buried Pipes in Unstable Sandy Slopes," *Landslides* 16, no. 2 (2019): 283–293.
21. J. R. M. S. Oliveira, K. I. Rammah, P. C. Trejo, M. S. S. Almeida, and M. C. F. Almeida, "Modelling of a Pipeline Subjected to Soil Mass Movements," *International Journal of Physical Modelling in Geotechnics* 17, no. 4 (2017): 246–256.
22. P. Tan, G. Chen, R. Huang, et al., "Surface Displacement Analysis of Rock Slope Based on Physical Simulation Tests," *Hydrogeology & Engineering Geology* 44, no. 04 (2017): 105–110.
23. Y. Zhang, H. Tang, G. Lu, et al., "Design and Testing of Inertial System for Landslide Displacement Distribution Measurement," *Sensors* 20, no. 24 (2020): 7154.
24. W. Feng, R. Huang, J. Liu, X. Xu, and M. Luo, "Large-Scale Field Trial to Explore Landslide and Pipeline Interaction," *Soils and Foundations* 55, no. 6 (2015): 1466–1473.
25. T. Xu, F. Xiong, F. Liao, Y. Li, and H. Jiang, "Method for Identifying the Main Factors Controlling Landslides Based on a Particle Coupling Algorithm Simulating the Ultimate State of a Gas Pipeline," *Computers and Geotechnics* 169 (2024): 106229.
26. F. Y. A, T. H. Chen, C. Yang, Y. F. Wu, and S. Q. Yan, "Study on Disaster Mechanism of Oil and Gas Pipeline Oblique Crossing Landslide," *Sustainability* 15, no. 4 (2023): 3012.
27. H. Wen, L. Liu, J. Zhang, J. Hu, and X. Huang, "A Hybrid Machine Learning Model for Landslide-Oriented Risk Assessment of Long-Distance Pipelines," *Journal of Environmental Management* 342 (2023): 118177.
28. Y. Liao, Y. Zhao, P. Li, et al., "Fracture Mechanics Analysis of Gas Pipeline With Circumferential Crack Under the Action of Transverse Landslide," *International Journal of Pressure Vessels and Piping* 209 (2024): 105199.
29. J. Zhang, X. Ma, J. Zhang, et al., "Insights Into Geospatial Heterogeneity of Landslide Susceptibility Based on the SHAP-XGBoost model," *Journal of Environmental Management* 332 (2023): 117357.
30. Y. Liao, C. Liu, T. Wang, et al., "Mechanical Behavior Analysis of Gas Pipeline With Defects Under Lateral Landslide," *Proceedings of the Institution of Mechanical Engineers Part C Journal of Mechanical Engineering Science*, 235, no. 23 (2021): 6752–6766.
31. X. Hao, W. Du, Y. Zhao, et al., "Dynamic Tensile Behaviour and Crack Propagation of Coal Under Coupled Static-Dynamic Loading," *International Journal of Mining Science and Technology* 30, no. 5 (2020): 659–668.
32. Q. Xu, R. Huang, et al, "Research Progress in Time Forecast and Prediction of Landslides," *Advance in Earth Sciences* 19, no. 3 (2004): 478–483.(in Chinese).
33. Q. Xu, M. Tang, et al, "Research on Space-Time Evolution Laws and Early Warning Prediction of Landslides," *Chinese Journal of Rock Mechanics and Engineering* 27, no. 6 (2008): 1104–1112 (in Chinese).